Parameter estimation in atomic spectroscopy using exceptional points

Morag Am-Shallem and Ronnie Kosloff
The Fritz Haber Research Center and The Institute of Chemistry, The Hebrew University, Jerusalem 91904, Israel

Nimrod Moiseyev
Schulich Faculty of Chemistry and Faculty of Physics, Technion, Haifa 3200008, Israel

(Received 27 December 2015; published 11 March 2016)

We suggest a method for accurate parameter estimation of atomic systems, employing the special properties of the exceptional points. The non-Hermitian degeneracies at the exceptional points emerge from the description of the spontaneous emission of the atomic system in the framework of an open quantum system, resulting in a non-Hermitian quantum master equation. The method is demonstrated for the atomic spectrum of $S \rightarrow P$ transitions of ^{85}Rb and $^{40}Ca^{+}$.

DOI: 10.1103/PhysRevA.93.032116

I. ELECTRONIC TRANSITIONS AND SPONTANEOUS EMISSION IN ATOMIC SYSTEMS

Atomic spectroscopy is unique in its experimental accuracy, able to achieve a dynamical range of precision of up to 18 significant digits. High-performance frequency standards are the technological result of this precision, leading to applications such as network synchronization and global positioning systems (GPS) [1]. This technology is enabled by atomic clocks [2,3]. High accuracy has implications in other fields of physics, such as radioastronomy (very-long-baseline interferometry) [4], tests of general relativity [5], and particle physics [6]. Atomic spectroscopy has been a primary source of fundamental constants [7]. For example, a small deviation of the Rydberg constant can indicate the radius of the proton [8].

A. Electronic transitions and spontaneous emission

Atomic spectroscopy is the study of electronic transition in atoms. The spectral lines correspond to Bohr frequencies of the transitions between energy levels of the atom. Within this viewpoint, the spectral theory involves calculating the eigenvalues of the atomic Hermitian Hamiltonian. The observed spectrum is then predicted by perturbation theory, assuming weak excitation and knowledge of the transition dipole matrix elements.

The simple picture of atomic spectroscopy is hampered by the notion that atoms are imbedded in the radiation field. The primary influence is spontaneous emission and Lamb shifts [9]. In principle, one can employ quantum field theory and treat the radiation field and the atom using a Hamiltonian description [10],

$$\hat{\mathbf{H}} = \hat{\mathbf{H}}_{\text{atom}} + \hat{\mathbf{H}}_{\text{radiation}} + \hat{\mathbf{H}}_{\text{interaction}}. \tag{1}$$

Our aim is to concentrate on the atomic spectra. We therefore employ a reduced description where we derive effective equations of motion for the atomic system by tracing out the radiation field. This is the approach incorporated in open quantum systems. In this case, the reduced dynamics is described by a non-Hermitian generator $\mathcal{L}$. We will show that due to non-Hermitian degeneracies, there is a profound and unexpected influence on the atomic spectrum.

B. The L-GKS equation for spontaneous emission

The phenomena of spontaneous emission (SE) cannot be described by a unitary description, such as the Schrödinger equation for the wave function, or the counterpart Liouville–von Neumann master equation for density matrices. Hamiltonian-based approaches incorporate only coherent dynamics. Dissipation and dephasing phenomena are properly described by the quantum master equation [11,12]. The general structure of the quantum master equation was introduced by Lindblad [13] and Gorini, Kossakowski, and Sudarshan [14] (L-GKS). Based on a mathematical construction, they obtained the general structure of the generator $\mathcal{L}$ of a completely positive dynamical semigroup. The L-GKS master equation (known also as the Lindblad equation) adds dissipative terms to the master equation which handles SE,

$$\frac{\partial \hat{\boldsymbol{\rho}}}{\partial t} = \mathcal{L}\hat{\boldsymbol{\rho}} = -\frac{i}{\hbar}[\hat{\mathbf{H}}, \hat{\boldsymbol{\rho}}] + \sum_{(a,b)} \Gamma_{a\rightarrow b} \times \left(\hat{\mathbf{A}}_{(a,b)}\, \hat{\boldsymbol{\rho}}\, \hat{\mathbf{A}}^{\dagger}_{(a,b)} - \frac{1}{2}[\hat{\mathbf{A}}^{\dagger}_{(a,b)}\hat{\mathbf{A}}_{(a,b)}, \hat{\boldsymbol{\rho}}]_{+} \right), \tag{2}$$

where $[\cdot,\cdot]$ denotes a commutator and $[\cdot,\cdot]_{+}$ denotes an anticommutator.

The first term is the commutator of the Hamiltonian with the density matrix, which generates the unitary dynamics. The second term is the dissipator, which generates the spontaneous emission. The sum is over the pairs of levels (a,b): Each of the annihilation operators

$$\hat{\mathbf{A}}_{(a,b)} \equiv \hat{\mathbf{A}}_{a\rightarrow b} = |b\rangle\langle a| \tag{3}$$

generates a decay from the upper source level $|a\rangle$ to the lower destination level $|b\rangle$. The anticommutator $[\hat{\mathbf{A}}^{\dagger}_{(a,b)}\hat{\mathbf{A}}_{(a,b)}, \hat{\boldsymbol{\rho}}]_{+}$ expresses the decrease in population of the excited state $|a\rangle$, while the resulting increase of population of the lower state $|b\rangle$ is expressed by the term $\hat{\mathbf{A}}_{(a,b)}\, \hat{\boldsymbol{\rho}}\, \hat{\mathbf{A}}^{\dagger}_{(a,b)}$. Note that the anticommutator contains the term

$$\hat{\mathbf{A}}^{\dagger}_{(a,b)}\hat{\mathbf{A}}_{(a,b)} = (|a\rangle\langle b|)(|b\rangle\langle a|) = |a\rangle\langle a| \equiv \hat{\mathbf{P}}_{a}, \tag{4}$$

where $\hat{\mathbf{P}}_a$ is the projection operator, projecting on the subspace spanned by $|a\rangle$. Therefore, the decrease in population of the excited state is expressed using only the population on this state and does not require knowledge of other states.

The decay rate for the pair of levels (b,a),$\Gamma_{a\to b}$ can be obtained by a microscopic derivation of the quantum optical master equation from the Hamiltonian of Eq. (1) under the weak-coupling limit. The Born-Markov approximation is employed where the perturbation parameter is the dipole interaction between the atom and the radiation at temperature $T=0$. The rate obtained is equivalent to the golden rule formula [15],

$$\Gamma_{a\to b}=\frac{4}{3}\frac{\omega_{ab}^3}{\hbar c^3}|d_{ab}|^2, \tag{5}$$

with ω_{ab} as the transition frequency, c the speed of light, and d_{ab} the transition dipole matrix element. For states with defined angular momentum, the transition dipole matrix element becomes

$$\Gamma_{a\to b}=\frac{4}{3}\frac{\omega_{ab}^3}{c^2}\alpha\frac{|\langle J_a||\hat{\mathbf{r}}||J_b\rangle|^2}{2J_b+1}. \tag{6}$$

Here, α is the fine-structure constant, and J_a, J_b are the angular momenta of the states $|a\rangle$ and $|b\rangle$. $\langle J_a||\hat{\mathbf{r}}||J_b\rangle$ is the reduced dipole matrix element between J_a and J_b.

The total decay rate from a state $|a\rangle$ is the sum $\Gamma_a=\sum_b\Gamma_{a\to b}$. This decay rate defines the lifetime of the excited state: $\tau_a=\Gamma_a^{-1}$.

The spontaneous-emission rate is completely determined by the fundamental physical constants: i.e., magnetic moment of the electron and the nuclei, etc. These constants determine the values of the energy level's splitting and lifetime. By inversion, an accurate measurement of the energies and lifetime constitutes an appropriate determination of universal parameters.

C. Population leakage

Typically, in atomic systems, the excitation and deexcitation transitions are not closed. Population can leak to other levels of the atomic system. The population is expressed by the diagonal entries in the density matrix $\hat{\boldsymbol{\rho}}$, and the total population is $\mathrm{Tr}\{\hat{\boldsymbol{\rho}}\}$. The dissipative term in Eq. (2) conserves the total population in the system, i.e., $\partial_t\,\mathrm{Tr}\{\hat{\boldsymbol{\rho}}(t)\}=0$. To incorporate population loss, we utilize the fact that the decrease of population in an excited state is described by the anticommutator terms, which use only the population on this state and do not require knowledge about other states. Therefore, the dissipator $\mathcal{L}$ will include additional terms composed only from the anticommutators. Such terms cause a decrease in the population of the excited state which are not compensated by an increase of population of other states. For each excited state $|a\rangle$, the additional term will have the form

$$\mathcal{L}_{\mathrm{leak}}^{(a)}\hat{\boldsymbol{\rho}}=-\tfrac{1}{2}\Gamma_{a,\mathrm{leak}}[\hat{\mathbf{P}}_a,\hat{\boldsymbol{\rho}}]_+. \tag{7}$$

The total decay rate from the state $|a\rangle$ is now $\Gamma_a=\Gamma_{a,\mathrm{leak}}+\sum_b\Gamma_{a\to b}$. We define $\chi_a=\Gamma_{\mathrm{leak}}/\Gamma_a$ as the *branching fraction* that decays from the excited state $|a\rangle$ to states out of the primary system. Introducing such leaking terms into the dissipator reduces the total population and, therefore, $\partial_t\,\mathrm{Tr}\{\hat{\boldsymbol{\rho}}(t)\}<0$.

The total spontaneous-emission part of the L-GKS equation will have the form

$$\begin{aligned}\mathcal{L}_{SE}\hat{\boldsymbol{\rho}}&=\sum_a\left\{\sum_b\Gamma_{a\to b}\left(\hat{\mathbf{A}}_{(a,b)}\,\hat{\boldsymbol{\rho}}\,\hat{\mathbf{A}}_{(a,b)}^\dagger-\frac{1}{2}[\hat{\mathbf{P}}_a,\hat{\boldsymbol{\rho}}]_+\right)\right.\\&\quad\left.-\frac{1}{2}\Gamma_{a,\mathrm{leak}}[\hat{\mathbf{P}}_a,\hat{\boldsymbol{\rho}}]_+\right\}\\&=\sum_a\left(\sum_b\Gamma_{a\to b}\hat{\mathbf{A}}_{(a,b)}\,\hat{\boldsymbol{\rho}}\,\hat{\mathbf{A}}_{(a,b)}^\dagger-\frac{1}{2}\Gamma_a[\hat{\mathbf{P}}_a,\hat{\boldsymbol{\rho}}]_+\right).\end{aligned} \tag{8}$$

If the excited state $|a\rangle$ decays to a manifold B with N_B states $|b\rangle\in B$ with equal decay rate, then we have $\Gamma_{a\to b}=(1-\chi_a)\Gamma_a/N_B$. The spontaneous-emission part will have the form

$$\mathcal{L}_{SE}\hat{\boldsymbol{\rho}}=\sum_a\Gamma_a\left\{\frac{(1-\chi_a)}{N_B}\sum_{b\in B}\hat{\mathbf{A}}_{(a,b)}\,\hat{\boldsymbol{\rho}}\,\hat{\mathbf{A}}_{(a,b)}^\dagger-\frac{1}{2}[\hat{\mathbf{P}}_a,\hat{\boldsymbol{\rho}}]_+\right\}. \tag{9}$$

D. Pure dephasing

Pure dephasing is the loss of coherence without change in population. Random fluctuations of the energy levels will generate pure dephasing. A possible mechanism is caused by elastic collisions with other atoms in the chamber. An additional mechanism is caused by noise in the monitoring or driving laser. As a result, the pure dephasing rate can be controlled, for example, by changing the density of the atomic gas or by generating fluctuations in the external field. We denote the pure dephasing rate by Γ_{deph}.

Within the L-GKS equation, pure dephasing is described by a generator $\mathcal{L}$ which commutes with the Hamiltonian, for example, $\mathcal{L}=\Gamma_{\mathrm{deph}}[\hat{\mathbf{H}},[\hat{\mathbf{H}},\cdot]]$.

E. The Heisenberg form

An alternative description is to describe the dynamics in an operator base. As a result, the L-GKS equation is employed in the Heisenberg representation [15–17], the Hermitian conjugate of Eq. (2). The equation of motion for an operator $\hat{\mathbf{X}}$ becomes

$$\begin{aligned}\frac{d}{dt}\hat{\mathbf{X}}&=\frac{\partial\hat{\mathbf{X}}}{\partial t}+\frac{i}{\hbar}[\hat{\mathbf{H}},\hat{\mathbf{X}}]\\&\quad+\sum_{(a,b)}\Gamma_{a\to b}\left(\hat{\mathbf{A}}_{(a,b)}^\dagger\hat{\mathbf{X}}\hat{\mathbf{A}}_{(a,b)}-\frac{1}{2}[\hat{\mathbf{P}}_a,\hat{\mathbf{X}}]_+\right).\end{aligned} \tag{10}$$

For a system with population leakage, the equation will have additional anticommutator terms, as in Eqs. (8) and (9).

II. DYNAMICS AT THE EXCEPTIONAL POINTS AND PARAMETER ESTIMATION

The dynamics generated by $\mathcal{L}$ will be represented by an explicit matrix vector notation. The density matrix $\hat{\boldsymbol{\rho}}$, which is an element in Liouville space, is represented as a vector,

while $\mathcal{L}$, which is a linear superoperator operating in this space, is represented by a matrix. There are a few methods to generate such a representation; cf. a recent demonstration in Ref. [17]. In this study, we employed the Heisenberg approach for the two-level systems and the "vec-ing" approach for larger systems. The vec-ing approach flattens the density matrix into a vector, representing the L-GKS generator by an appropriate matrix. This results in $N^2 \times N^2$ matrices for the L-GKS generator. We denote the vector representation of the density matrix $\hat{\boldsymbol{\rho}}$ as $\vec{\rho}$ and the matrix representation of $\mathcal{L}$ by L. In this notation, Eq. (2) is expressed by a matrix-vector equation,

$$\dot{\vec{\rho}} = L\vec{\rho}. \tag{11}$$

The eigenvalues of the matrix L reflect the non-Hermitian dynamics generated by $\mathcal{L}$. In general, they are complex, with the steady-state eigenvector having an eigenvalue of zero.

A. L-GKS dynamics and exceptional points

The solution for Eq. (2), given an initial density matrix $\hat{\boldsymbol{\rho}}_0$ and assuming that the generator $\mathcal{L}$ is time independent, can be formally expressed by

$$\hat{\boldsymbol{\rho}}(t) = e^{\mathcal{L}t}\hat{\boldsymbol{\rho}}_0. \tag{12}$$

In the matrix-vector representation, we have

$$\vec{\rho}(t) = e^{Lt}\vec{\rho}(0). \tag{13}$$

The dynamics described by Eq. (13) typically is described by a sum of decaying oscillatory exponentials. The dynamics of expectation values of operators, as well as other correlation functions, will have the analytical form (see Appendix A)

$$\langle X(t)\rangle = \sum_k d_k \exp[-i\omega_k t], \tag{14}$$

where $-i\omega_k$ are the eigenvalues of L,d_k are the associated amplitudes, and both ω_k and d_k can be complex.

The spectrum of the non-Hermitian matrix L is a function of the external parameters of the system. For specific values, the spectrum becomes incomplete. This is due to the coalescence of several eigenvectors, denoted as a non-Hermitian degeneracy. For such parameters, the matrix L is not diagonalizable. Such points in the parameter space are known as *exceptional points* (EPs). At the exceptional point, the dynamics has a polynomial character. The temporal value of expectation values of operators has the form

$$\langle X(t)\rangle = \sum_k \sum_{\alpha=0}^{r_k} d_{k,\alpha} t^\alpha \exp\left[-i\omega_k^{(r_k)} t\right], \tag{15}$$

which replaces the form of Eq. (14) (see Appendix A).

When two eigenvalues of the master equations coalesce into one, a second-order non-Hermitian degeneracy is obtained. We refer to it as a second-order exceptional point and denote it with EP2. A third-order non-Hermitian degeneracy is denoted by EP3. There are points in the parameter space in which n pairs of eigenvectors coalesce, each pair coalesces into a distinct eigenvector. They will be denoted as EP2^n.

B. Identification of EPs using the dynamics

The analytical form of decaying exponentials, given by Eq. (14), is used in harmonic inversion methods to find the frequencies and amplitudes of the time-series signal [18–20]. Harmonic inversion methods are widely used for the analysis of experiments in diverse fields such as NMR spectroscopy [21], Fourier-transform mass spectrometry [22], and ultrafast pump-probe molecular spectroscopy [23].

However, at exceptional points, the analytical form is different: Fuchs *et al.* showed that applying standard harmonic inversion methods, which were designed for Eq. (14), to a signal generated by Eq. (15) leads to divergence of the amplitudes d_k [24]. We used the Padé approximant harmonic inversion algorithm presented in Refs. [20,24]. The divergence of the amplitudes d_k in the vicinity of exceptional points is employed to accurately locate them in the parameter space [24,25].

C. Parameter estimation using EPs

The ability to accurately locate the EPs in the parameter space is used for parameter estimation. The procedure is as follows.

(1) Accurately locate in the parameter space the desired exceptional point by iterating the following steps:

(a) Perform an experiment to obtain a time series of a physical observable.

(b) Obtain the characteristic frequencies and amplitudes of the signal.

(c) In the parameter space, estimate the direction and distance to the EP and determine new parameters for the next iteration.

(2) At the EP, invert the relations between the characteristic frequencies and the system parameters to obtain the system parameters.

The accurate location of the exceptional points, followed by inverting the relations, will lead to an accurate parameter estimation. This procedure was used to estimate the parameters of the Bloch system from iterations of time series [25]. This parameter estimation is robust to uncertainties in the location of the EPs. The noise sensitivity is affected by the harmonic inversion. See a short discussion regarding noise in harmonic inversion methods in Appendix C.

III. PARAMETER ESTIMATION OF EFFECTIVE TWO-LEVEL SYSTEMS

A. Closed two-level systems

Under the influence of polarized driving fields, some atomic transitions behave as a closed two-level system. An example is the transition between the hyperfine states $|5^2S_{1/2}, F = 3, m_F = 3\rangle$ and $|5^2P_{3/2}, F = 4, m_F = 4\rangle$ of the ^{85}Rb atom, with σ^+ polarization. The selection rules impose that all of the transitions—stimulated and spontaneous—occur only between these states. The system parameters are system frequency of $\omega_s = 384.229\,241\,689$ THz (assuming no Zeeman splitting), decay rate of $\Gamma = 38.117 \times 10^6\ \mathrm{s}^{-1}$, and dipole moment of $\mu = 2.98931\ ea_0$ [26]. We define the detuning between the system frequency ω_s and the electromagnetic

field carrier frequency ω_s as $\Delta = \omega_s - \omega_L$. The resonance Rabi frequency is $\Omega_R = -\mu E_0/\hbar$, where E_0 is the amplitude of the electromagnetic field.

We employ the Heisenberg representation to describe the dynamics. We define $|s\rangle$ as the lower state and $|p\rangle$ as the upper state. The dynamics are described by the set of operators,

$$\begin{aligned}\hat{\mathbf{X}} &\equiv |s\rangle\langle p| + |p\rangle\langle s|,\\ \hat{\mathbf{Y}} &\equiv i(|s\rangle\langle p| - |p\rangle\langle s|),\\ \hat{\mathbf{Z}} &\equiv |p\rangle\langle p| - |s\rangle\langle s|,\\ \hat{\mathbf{I}} &\equiv |p\rangle\langle p| + |s\rangle\langle s|.\end{aligned} \tag{16}$$

We form a four vector from these operators. We write the Heisenberg equations, given by Eq. (10), for the operators in this vector and get a differential equation with a 4×4 matrix [17]. The conservation of population is expressed by $\frac{d}{dt}\hat{\mathbf{I}} = 0$. Therefore, we can omit the equation for the operator $\hat{\mathbf{I}}$ and add an inhomogeneous term instead. This results in the Bloch equations [25]. To find the exceptional points, we need only the homogeneous part of the equation, which is incorporated in the matrix

$$\mathrm{M} = \begin{pmatrix} -\frac{\Gamma}{2} & \Delta & 0 \\ -\Delta & -\frac{\Gamma}{2} & \Omega_R \\ 0 & -\Omega_R & -\Gamma \end{pmatrix}. \tag{17}$$

The EPs of this matrix compose a deltoidlike curve. The curve is demonstrated in Fig. 1 (i.e., the $\chi = 0$ curve; the other curves in this figure refer to systems with population leakage and will be described below). The cusps of this EP curve are identified as EP3. The accurate location of the EP3 can be used to estimate the parameters of such systems, as described in Sec. II C above and in a previous study [25].

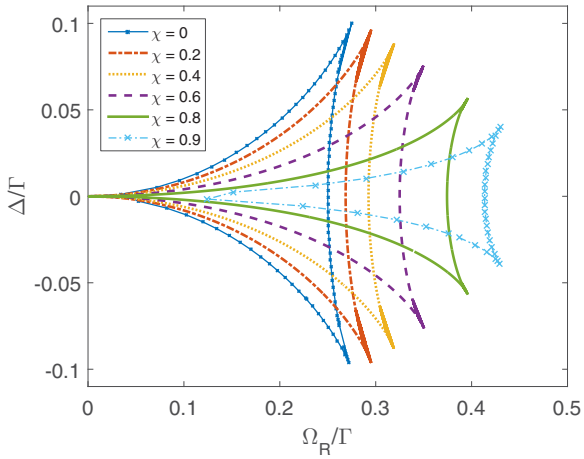

FIG. 1. A map of the Bloch-like EP curves of the matrix in Eq. (19), which describes the dynamics of a two-level system with spontaneous emission, when some of the excited population decays out of the system, with χ as the branching fraction. Figure in scaled coordinates could correspond to any leaking TLS such as Rb or Ca^+. The curves are twofold non-Hermitian degeneracy (EP2). The curves merge into cusps which are identified as EP3. The map of the EP curves can be used for estimation of the system parameters: the system frequency, the decay rate, and the branching fraction.

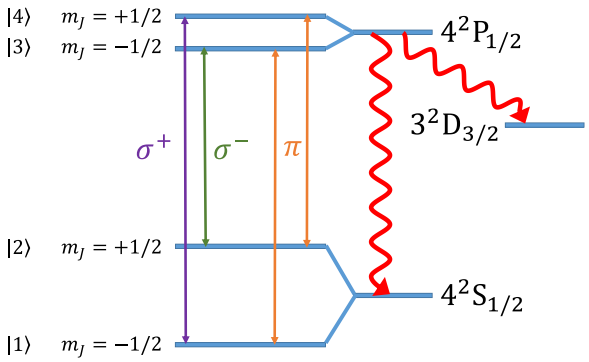

FIG. 2. A scheme of the relevant energy levels in $^{40}Ca^+$. The $^2S_{1/2}$ and $^2P_{1/2}$ orbitals have total angular momentum of $j = \frac{1}{2}$. They are split by magnetic field two sublevels of $m_j \pm \frac{1}{2}$. External electromagnetic fields with σ^+ and σ^- circular polarizations induce $\Delta m = +1$ and $\Delta m = -1$ transitions, respectively. Linearly polarized electromagnetic fields (π polarization) induce $\Delta m = 0$ transitions. The excited population at the $^2P_{1/2}$ state spontaneously decays to the $^2S_{1/2}$ and $^2D_{3/2}$ states. Energy levels are not to scale.

B. Two-level systems with population leakage

The Bloch equation can be extended to include SE that leaks into states that are external to the Hamiltonian, resulting in population loss; see Sec. I C above. Here are two examples for such systems:

(i) *Rubidium atom*. Consider the two-level system (TLS) composed by the two hyperfine states $|5^2S_{1/2}, F = 3, m_F = 2\rangle$ and $|5^2P_{3/2}, F = 3, m_F = 3\rangle$ of the ^{85}Rb atom [26], with σ^+ polarization. The selection rules impose stimulated transitions between these states, but the excited state, $|5^2P_{3/2}, F = 3, m_F = 3\rangle$, decays spontaneously also to other states in the system. Under σ^+ polarization, there are no transitions from these other states back to the TLS. Therefore, we can treat this system as a TLS with population loss.

(ii) *Calcium ion*. Consider the TLS composed by the two states $|4^2S_{1/2}, m_J = -1/2\rangle$ and $|4^2P_{1/2}, m_J = 1/2\rangle$ of the $^{40}Ca^+$ ion, with σ^+ polarization (cf. Sec. IV B and Fig. 2 below). Again, there are stimulated transitions between these states, but the excited states also decay to $|3^2D_{3/2}\rangle$ states ($\approx$6.5% of the decay rate) and to the state $|4^2S_{1/2}, m_J = 1/2\rangle$ (50% of the remaining decay rate). The population on these states does not revert to the TLS [27].

The Heisenberg equation in this case [cf. Eq. (9) with $N_B = 1$ and Eq. (10)] is

$$\frac{d}{dt}\hat{\mathbf{O}} = \frac{i}{\hbar}[\hat{\mathbf{H}}, \hat{\mathbf{O}}] + \Gamma\left\{(1-\chi)\hat{\mathbf{S}}_+\hat{\mathbf{O}}\hat{\mathbf{S}}_- - \frac{1}{2}[\hat{\mathbf{S}}_+\hat{\mathbf{S}}_-, \hat{\mathbf{O}}]_+\right\}. \tag{18}$$

Here, Γ is the total decay rate of the excited state. It is the sum of the decay rate into the lower level $|s\rangle$, as in Eq. (10) above, and of the decay rate out of the system, as in Eq. (7). χ is the branching fraction that decays to states out of the primary system. $\hat{\mathbf{S}}_+ \equiv |p\rangle\langle s|$ and $\hat{\mathbf{S}}_- \equiv |s\rangle\langle p|$ are the raising and lowering operators. We write the equations for the four operators of Eq. (16). In this case, $\frac{d}{dt}\hat{\mathbf{I}} \neq 0$ and we cannot omit

the equation for this operator. The resulting set of equations is

$$\frac{d}{dt}\begin{pmatrix}\hat{\mathbf{X}}\\ \hat{\mathbf{Y}}\\ \hat{\mathbf{Z}}\\ \hat{\mathbf{I}}\end{pmatrix}=\begin{pmatrix}-\frac{1}{2}\Gamma & \Delta & 0 & 0\\ -\Delta & -\frac{1}{2}\Gamma & \Omega_R & 0\\ 0 & -\Omega_R & -\left(1-\frac{\chi}{2}\right)\Gamma & -\left(1-\frac{\chi}{2}\right)\Gamma\\ 0 & 0 & -\frac{\chi}{2}\Gamma & -\frac{\chi}{2}\Gamma\end{pmatrix}\times\begin{pmatrix}\hat{\mathbf{X}}\\ \hat{\mathbf{Y}}\\ \hat{\mathbf{Z}}\\ \hat{\mathbf{I}}\end{pmatrix}. \tag{19}$$

The EPs of this matrix compose a deltoid curve, with χ-dependent shape. Figure 1 shows EP curves for different values of χ. The EP curve and the time series of the driven system can be used for accurate parameter estimation:

(a) The total decay rate Γ can be calculated from the eigenvalues of the matrix in Eq. (19): the sum of the eigenvalues is always 2Γ.

(b) The transition frequency is found by the locations of the EPs at small amplitudes of the driving field.

(c) The branching fraction χ of a given system can be found by fitting the shape of the EP curve to the appropriate branching fraction.

IV. EPs IN THE H LINE OF THE CALCIUM ION AND PARAMETER ESTIMATION

A. The $^{40}Ca^{+}$ ion

The ^{40}Ca is the most abundant calcium isotope. The total spin of the ^{40}Ca nucleus vanishes. The ground state of the $^{40}Ca^{+}$ ion includes 18 electrons in closed shells, and the remaining single electron occupying the lower orbital of the 4th shell. Therefore, the $^{40}Ca^{+}$ ion is isoelectronic to alkali metals. However, since the total spin of the nucleus vanishes, there is no hyperfine structure.

The structure of the energy levels of the $^{40}Ca^{+}$ ion has been found to be suitable for many applications. In particular, $^{40}Ca^{+}$ has been used in the field of quantum computing and quantum information [28–33], for atomic clocks and the frequency standard [1–3,34–37], and, recently, as a single-atom heat engine [38]. The spectrum of $^{40}Ca^{+}$ has also been employed in the quest for drifts of the fine-structure constant over a time span of many billion years [39,40].

B. The H transition of the $^{40}Ca^{+}$ system

At the ground electronic state, the electron occupies the orbital $4s$, with an orbital angular momentum $l=0$. The total angular momentum including the electron spin becomes $j=\frac{1}{2}$. The spectroscopic notation for the ion at this state is $4^2S_{1/2}$. At the first excited electronic state, the electron occupies the orbital $4p$, with an orbital angular momentum $l=1$. This state has a fine-structure splitting due to spin-orbit coupling either $j=\frac{1}{2}$ (denoted as $4^2P_{1/2}$) or $j=\frac{3}{2}$ (denoted as $4^2P_{3/2}$).

The transition from $4^2S_{1/2}$ to $4^2P_{1/2}$ is known as the H line. The transition from $4^2S_{1/2}$ to $4^2P_{3/2}$ is known as the K line. These terms stem from the study of the solar spectrum. In the following, we concentrate on the H line, i.e., the $4^2S_{1/2}\Leftrightarrow 4^2P_{1/2}$ transition. The frequency of this transition was measured to be 755 222 766.2(1.7) MHz [39]. The $4^2P_{1/2}$ has a lifetime of $\tau\approx 7$ ns and it spontaneously decays back to the $4^2S_{1/2}$ state, as well as to the $3^2D_{3/2}$ state. The branching between these two decays is $\Gamma_{P\to S}\approx 0.935\times\Gamma_{\text{total}}$. We treat the decay into the $3^2D_{3/2}$ state as leakage out of the system, with $\chi=1-0.935=0.065$. Each of the states $4^2S_{1/2}$ and $4^2P_{1/2}$ is twofold degenerated, with sublevels of $m_j=\pm\frac{1}{2}$. When an external magnetic field is applied, the Zeeman effect removes degeneracies. The magnetic-field-dependent shift in the transition frequency is ± 19 kHz/μT for the $\Delta m=\pm 1$ transitions (i.e., the transitions that are induced by circularly polarized electromagnetic fields) [39]. This shift is the sum of two contributions: the decrease of energy of the lower sublevel of the $S_{1/2}(\approx 75\%)$ and the increase of the upper sublevel of the $P_{1/2}(\approx 25\%)$. The ratio is determined by the appropriate Landé factors. For a linearly polarized electromagnetic field, $\Delta m=0$ transitions are induced. Therefore, we expect to obtain only half of the above shift, i.e., ± 9.5 kHz/μT. However, in weak magnetic fields, this shift is obscured by the natural linewidth in the standard frequency-domain spectroscopy (see Ref. [39], for example). A scheme of the relevant energy levels is presented in Fig. 2.

C. The system model

The energy level's structure and the spontaneous emission of the $^{40}Ca^{+}$ ion system allow the use of EPs in the task of parameter estimation. The reduced system Hamiltonian includes four levels (see Fig. 2 for a sketch of these levels). The $4^2S_{1/2}$ sublevels are denoted as $|1\rangle$ and $|2\rangle$, and the $4^2P_{1/2}$ sublevels are denoted as $|3\rangle$ and $|4\rangle$. The rotating-wave Hamiltonian, under the influence of an oscillating electromagnetic field of detuning Δ and amplitude Ω_R, and under a constant magnetic field which induces a split of ω_{21} between the two $S_{1/2}$ sublevels, and a split of ω_{43} between the two $P_{1/2}$ sublevels, is

$$\hat{\mathbf{H}}_0=\hbar\begin{pmatrix}\frac{1}{2}(\omega_{43}-\Delta) & 0 & \Omega_R & 0\\ 0 & \frac{1}{2}(-\omega_{43}-\Delta) & 0 & \Omega_R\\ \Omega_R & 0 & \frac{1}{2}(\omega_{21}+\Delta) & 0\\ 0 & \Omega_R & 0 & \frac{1}{2}(-\omega_{21}+\Delta)\end{pmatrix}. \tag{20}$$

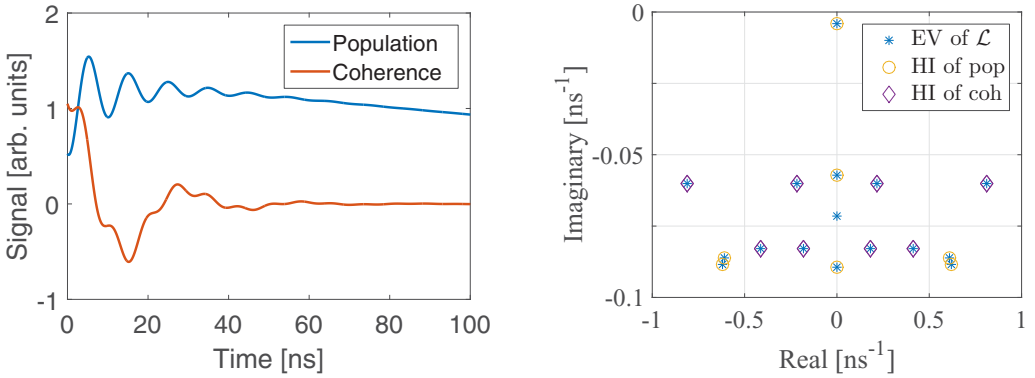

FIG. 3. Left panel: An example of two emission time signals of Ca^+, obtained by simulating the dynamics of the populations $\hat{\mathbf{O}}_{\text{pop}}$ and the coherences $\hat{\mathbf{O}}_{\text{coher}}$ (see definitions in text). The initial state is the steady state with repumping lasers switched on. The transient dynamics is initiated by turning the pumping laser off. The time interval in this figure, 100 ns, reflects the population decay lifetime, $\tau_{\text{population}} \approx 108$ ns. Right panel: The locations in the complex plane of the complex frequencies that were obtained from these signals using harmonic inversion (HI). The actual eigenvalues of the generator $\mathcal{L}$ are marked with asterisks. Different subsets of the generator eigenvalues were obtained for different signals. The frequencies of the population signal are marked by circles, while the frequencies of the coherence signal are marked by diamonds.

The spontaneous emission is incorporated into the dynamics by the dissipative part of the L-GKS equation, as described in Sec. I B above. We used the operators

$$\hat{\mathbf{A}}_{p\to s} \equiv |s\rangle\langle p|, \tag{21}$$

where $|s\rangle$ denotes the states of the two lower levels, $|1\rangle$ and $|2\rangle$, and $|p\rangle$ denotes the states of the upper levels, $|3\rangle$ and $|4\rangle$. This results in four terms in the dissipator, where each of the $P_{1/2}$ sublevels decays to each of the $S_{1/2}$ sublevels, with rate of $\Gamma_{P_i\to S_k} = \frac{1}{2}\Gamma_{(P\to S)_{\text{total}}} = \frac{1-\chi}{2}\Gamma_{\text{total}}$. Another two terms describe the decay from the $P_{1/2}$ sublevels to the $D_{3/2}$ state, using only the anticommutator terms as shown in Eq. (7), with the decay rate of $\Gamma_{P\to D} = \chi\Gamma_{\text{total}}$. These dynamical terms are incorporated in $\mathcal{L}$, leading to the dynamical equation for the 4×4 density matrix $\hat{\boldsymbol{\rho}}$:

$$\frac{\partial}{\partial t}\hat{\boldsymbol{\rho}} = \mathcal{L}\hat{\boldsymbol{\rho}} = -\frac{i}{\hbar}[\hat{\mathbf{H}}_{\mathbf{0}}, \hat{\boldsymbol{\rho}}] + \sum_{p\in \mathrm{P}_{1/2}} \Gamma_{\text{total}} \times \left\{ \frac{(1-\chi)}{2} \sum_{s\in \mathrm{S}_{1/2}} \hat{\mathbf{A}}_{(p,s)}\,\hat{\boldsymbol{\rho}}\,\hat{\mathbf{A}}^{\dagger}_{(p,s)} - \frac{1}{2}[\hat{\mathbf{P}}_p, \hat{\boldsymbol{\rho}}]_+ \right\}. \tag{22}$$

D. Locations of the EPs and parameter estimation

Our task is to find the exceptional points, which are the non-Hermitian degeneracies of the L-GKS generator of Eq. (22). Experimentally, the first step is to obtain a time series from the driven system. As an example, we mimic a possible experiment by simulating the time series of the emission signal by solving Eq. (22). The initial condition is obtained by first setting the laser detuning and amplitude to obtain the steady state. To overcome the population leakage, two examples for such measurable observables are the populations of the excited states, $\hat{\mathbf{O}}_{\text{pop}} \equiv |3\rangle\langle 3| + |4\rangle\langle 4|$, and the coherences between these states, $\hat{\mathbf{O}}_{\text{coher}} \equiv |3\rangle\langle 4| + |4\rangle\langle 3|$. The population from $D_{3/2}$ is repumped to $P_{1/2}$ using an auxiliary laser. After a steady state is reached, the auxiliary laser is turned off, obtaining $\hat{\boldsymbol{\rho}}(0)$. The decay signal is now collected from $\hat{\boldsymbol{\rho}}(t)$ for a particular observable in an ordered time grid. The left panel of Fig. 3 shows an example for such time signals. The time series is the input for the harmonic inversion, which extracts the frequencies and amplitudes of the time signal. The frequencies are determined by the system parameters, while the initial state $\hat{\boldsymbol{\rho}}(0)$ determines the amplitudes. The right panel of Fig. 3 shows the obtained frequencies in the complex plane. The time interval in this figure is 100 ns, reflecting the population decay lifetime, $\tau_{\text{population}} = \tau_{SE}/\chi \approx 108$ ns. To map the EP at the parameter space, this procedure is repeated for other values of the laser detuning and amplitude.

For any such parameter set defining $\mathcal{L}$, the sum of the 16 eigenvalues of $\mathcal{L}$ can be shown to be $\sum_{k=1}^{16}\omega_k = 8\Gamma_{\text{total}}$. A similar relationship was obtained for the two-level system, where the sum of the four eigenvalues is 2Γ.

The task is to calculate the expected locations of the exceptional points of Eq. (22) in the parameter space of the amplitude and detuning. We used the method of fixed relative distance (MFRD) and the eigenvalues condition number methods for this task (see Appendix B and Refs. [41,42]). The map of EP curves is shown in Fig. 4 for the $^{40}Ca^+$ ion, with Zeeman splitting of 200 MHz. Note the gaps in the y axis. The resulting EP curves of the four-level system are more involved than the two-level case. In principle, there could be very high-order non-Hermitian degeneracies of Eq. (22). In practice, we found few EP curves of second-order degeneracy, and two other fourth-order EPs.

Close to each of the resonances between the upper and lower levels, there is an EP curve which is similar to the deltoid EP curve we got for the Bloch system [25]. The exact frequency of the resonances can be found by locating pairs of EPs with detunings above and below the resonance, while maintaining a fixed amplitude. The shape of the curves can be fitted to estimate the branching ratio.

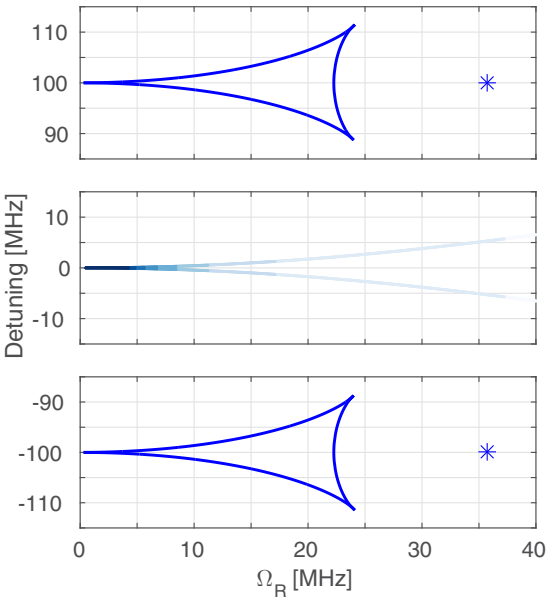

FIG. 4. A map of the EP curves of $^{40}Ca^{+}$ ion [Eq. (22)], with Zeeman splitting of 200 MHz, under linearly polarized driving field. Each of the Bloch-like curves (compare to the Bloch curves in Fig. 1) is found on a resonance between a pair of sublevels, one from $4\,^2S_{1/2}$ and one from $4\,^2P_{1/2}$. Note the gaps in the y axis of the different curves. To the right of each of the Bloch-like EP curves, there is a point of EP2^4 (marked with asterisks), in which four pairs of eigenvectors coalesce into four distinct eigenvectors. The detuning at these points is the splitting of the relevant resonance. The amplitude is $\Omega_R = \frac{1}{4}\Gamma_{\text{total}}$. Between the two Bloch-like EP curves, at the detuning $\Delta = 0$, which is the H-line transition frequency, there is a degeneracy curve of the L-GKS generator. It is not decisive whether this curve is an EP curve.

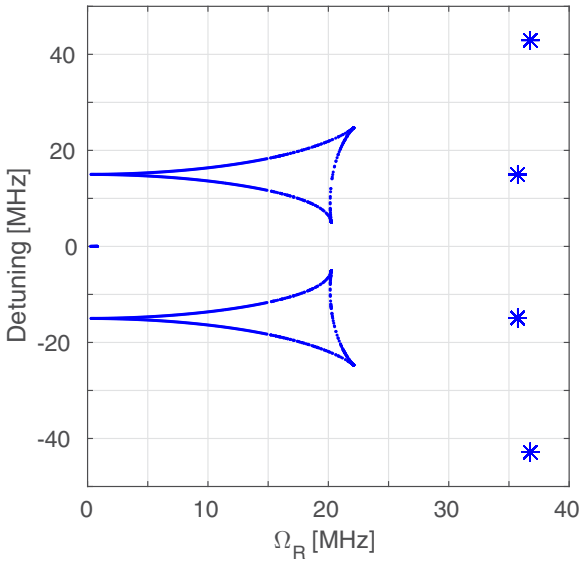

FIG. 5. A map of the EP curves of the $^{40}Ca^{+}$ ion [Eq. (22)], with Zeeman splitting of 30 MHz. The general structure is similar to the case of 200 MHz splitting (Fig. 4), but the Bloch-like curves get closer and interfere. The interference leads to skewing of these curves. The EP2^2 still can be located and employed for parameter estimation. Another two isolated EP2^2 can be seen at the right corners.

These resonance frequencies can be verified by locating the distinct EPs on the right of the Bloch-like curves (see Fig. 4). These two isolated points are classified as EP2^4, i.e., coalescence of four pairs of eigenvectors with four distinct eigenvalues. Each of these points is located with detuning Δ at the same frequency as the resonance, and amplitude of $\Omega_R = \frac{1}{4}\Gamma_{\text{total}}$. These points can also be used to extract the total decay rate Γ.

Between the two Bloch-like EP curves, in the $4\,^2S_{1/2} \Leftrightarrow 4\,^2P_{1/2}$ transition frequency, there is a curve of degeneracy points. However, we could not determine whether these degeneracies are exceptional points. Anyway, locating these degeneracies can be employed for determining the transition frequency.

To summarize, the suggested procedure for parameter estimation which includes four transition frequencies, laser driving power, spontaneous-emission rate, and leakage is as follows:

(1) The sum of the 16 frequencies obtained by the harmonic inversion of the time signal can be used to estimate the total spontaneous-emission rate: $\sum_{k=1}^{16}\omega_k = 8\Gamma_{\text{total}}$.

(2) The locations of the Bloch-like curves are used for the estimation of the frequencies of the resonances between the Zeeman sublevels.

(3) The shapes of the Bloch-like curves are used for the estimation of the branching ratio (in particular the EP3 points).

(4) The locations of the EP2^4 points are used to verify the resonances frequencies and the decay rate.

(5) The location of the degeneracy curve between the Bloch-like curve is used to estimate the H-line transition frequency.

Repetition of this procedure for various magnitudes of the external magnetic field can be used to trace the Zeeman and Paschen-Back effects.

For small external magnetic field, the Bloch-like curves approach each other and interfere. The shape of these curves is then skewed. This is demonstrated in Fig. 5, which shows the map of EP curves for the $^{40}Ca^{+}$ ion, with Zeeman splitting of 30 MHz. However, the resonances frequencies can be estimated using the locations of the EPs at small amplitudes, and verified by the location of the isolated EP2^4 points. In addition to those EP curves and points, we observed two other isolated EP2^2, at larger detuning and slightly larger amplitude. We did not find exact analytical expressions for these points.

E. Dependency of the EPs on other dephasing rates

Most of the sources for pure dephasing of laser-driven atomic spectroscopy are well controlled experimentally, for example varying the density of the ion gas or the medium gas, or the instrument noise in the laser amplitude and frequency. Care must be taken when analyzing EP curves in atomic spectra to get the relaxation rate Γ, since the rate depends on the various relaxation and dephasing rates in the system. For example, in the Bloch equations, if the spontaneous emission rate is Γ_{SE} and pure dephasing rate is Γ_{PD}, then the relaxation rate that appears in the matrix of Eq. (17) is $\Gamma = \Gamma_{SE} - \Gamma_{PD}$ [25].

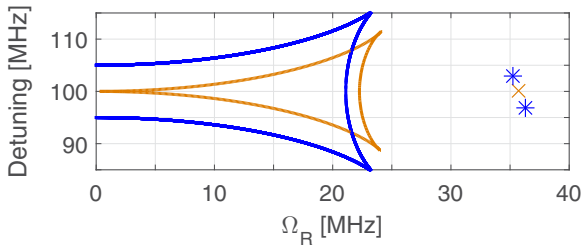

FIG. 6. A map of the upper EP curve of the driven $^{40}Ca^{+}$ ion with Zeeman splitting of 200 MHz and noise in the laser amplitude [Eq. (22) with additional double commutator with $\hat{\mathbf{V}}_{\text{deph}}$ term, defined in Eq. (23)]. Blue line: The EP curve for dissipation rate of $\Gamma_{\text{deph}} = 0.01$ ns^{-1}, along with the associated two EP2^2 (blue asterisks). The orange dashed line and "x" are the EP curve and the EP2^4 obtained for the noiseless case ($\Gamma_{\text{deph}} = 0$ ns^{-1}), shown in Fig. 4. For the case of $\Gamma_{\text{deph}} = 0.01$ ns^{-1}, the two branches do not merge at a small amplitude. Instead, they are split symmetrically around the resonance. The splitting magnitude is equal to the dephasing rate Γ_{deph}. In addition, the added dephasing splits the EP2^4 of the noiseless case into two distinct EP2^2s.

Generally, every noise source that can be added to the L-GKS equation is reflected by the complex eigenvalues of the generator $\mathcal{L}$. These eigenvalues are complex frequencies of the time signal. Therefore, the noise source can be traced by the harmonic inversion. The noise will result in changes in the EP-curve map. The experimental noise will influence only the harmonic inversion. See Appendix C for a short discussion regarding noise in harmonic inversion methods.

As an example, the influence of noise in the amplitude of the driving laser was analyzed. Such a noise is modeled in the L-GKS equation by a double commutator with the laser amplitude operator $\hat{\mathbf{V}}_{\text{deph}}$, which commutes with the Ω_R amplitude part of the Hamiltonian,

$$\hat{\mathbf{V}}_{\text{deph}} = \sqrt{\frac{1}{2}}\begin{pmatrix} 0 & 0 & 1 & 0 \\ 0 & 0 & 0 & 1 \\ 1 & 0 & 0 & 0 \\ 0 & 1 & 0 & 0 \end{pmatrix}. \tag{23}$$

The dissipation generated by the double commutator with this operator is not pure dephasing since it also generates relaxation.

We calculated the EP map in the parameter space for the dissipation rate of $\Gamma_{\text{deph}} = 0.01$ ns^{-1} with Zeeman splitting of 200 MHz. The upper Bloch-like EP curve of the results is presented in Fig. 6, along with the associated two EP2^2. For comparison, the upper curve of the noiseless case (presented in Fig. 4) is also shown. Two prominent differences can be found. The first is that the two branches do not merge at a small amplitude. Instead, they are split symmetrically around the resonance. The splitting magnitude is equal to the dephasing rate Γ_{deph}. The second difference is the splitting of the EP2^4 into two distinct EP2^2s. This splitting is not symmetric; therefore we cannot deduce the system parameters from the locations of these EP2^2s.

V. DISCUSSION

The irreversible character of the L-GKS equation is well known and indicated by the semigroup character of the evolution operator [15,43–45]. The generator of the dynamics $\mathcal{L}$ is therefore non-Hermitian. This means that non-Hermitian degeneracies EPs play an important role in open quantum systems.

So far, EPs were studied in the coalescence of two resonances. The resonances were metastable states associated with predissociation or autoionization phenomena and with leaking modes in waveguides [46,47]. A theoretical quest for multiple EPs [48], or for high-order EPs in dissipative physical systems, is pursued [49–52], specifically in the spectra of atoms in external fields [53].

The first study of EPs in the context of the L-GKS equation was for the simple two-level system described by the Bloch equations [25]. In the present study, we generalize to an open two-level system where population can leak out. Then we extend to a four-level system where the splitting can be controlled by a magnetic field. We found a rich and fascinating structure of EPs and EP curves, including higher-order EPs. Such phenomena is expected for many other open quantum systems described by the L-GKS equation.

The methods developed pave the way for a generic framework of employing EPs for parameter estimation of atomic systems. The dynamics near the EPs has enhanced sensitivity due to their analytic properties: small changes in the parameters lead to different harmonic inversion. Therefore, for parameter estimation, the harmonic inversion at the EPs is superior to standard inversion methods.

The first stage is to predict the EP map of the system: The state of an atom driven by a cw laser can be described in the rotating frame by a time-independent L-GKS equation. The parameter space for such a L-GKS generator contains the field amplitude and the detuning frequency. Such a parameter space can be scanned using the MFRD method to find the approximate locations of degeneracies of the generator. The location and character of these degeneracies are then examined using the condition number of the eigenvalues to identify and locate the EPs. The second stage is to search for the predicted EPs experimentally: The time signals obtained from the experiments are analyzed using harmonic inversion. The resulting frequencies and amplitudes are then used to find the degeneracies and exceptional points. Finally, we estimate the system parameters by comparing the predicted and the experimental EPs.

An interesting different system for an EP search can be two molecular electronic surfaces, with vibrational relaxation. A simple model for such a system can include only four levels [54], or even three: one level from the ground state and two vibrational levels from the excited state. Such systems can have multiple steady states and therefore can possess richer dynamics.

ACKNOWLEDGMENTS

We thank Ido Schaefer, Amikam Levy, and Raam Uzdin for fruitful discussions. We also thank A. L. Wolf, W. Ubachs, and K. S. E. Eikema for their help on the Ca^{+} system. We thank P. Gould for his advice. This work was supported by the Israel

Science Foundation Grants No. 2244/14 and No. 298/11 and by I-Core: the Israeli Excellence Center "Circle of Light."

APPENDIX A: DYNAMICAL SIGNATURE OF THE EPs

The solution for the L-GKS equation in the matrix-vector representation, given by Eq. (11), is

$$\vec{\rho}(t) = e^{Lt}\vec{\rho}(0). \tag{A1}$$

When L is diagonalizable, we can write $L = T\Lambda T^{-1}$, for a nonsingular matrix T and a diagonal matrix Λ, which has the eigenvalues $\{\lambda_i\}$ on the diagonal. Then we have

$$e^{Mt} = Te^{\Lambda t}T^{-1}. \tag{A2}$$

The matrix $e^{\Lambda t}$ is a diagonal matrix, which has the exponential of the eigenvalues, $\exp[\lambda_i t]$, on its diagonal. The resulting dynamics of expectation values of operators, as well as other correlation functions, follows a sum of decaying oscillatory exponentials. The analytical form of such dynamics is

$$\langle X(t)\rangle = \sum_k d_k \exp[-i\omega_k t], \tag{A3}$$

where $-i\omega_k$ are the eigenvalues of L,d_k are the associated amplitudes, and both ω_k and d_k can be complex.

For special values of the system parameters, the spectrum of the non-Hermitian matrix L is incomplete. This is due to the coalescence of several eigenvectors, referred to as a non-Hermitian degeneracy. The difference between Hermitian degeneracy and non-Hermitian degeneracy is essential: In the Hermitian degeneracy, several different orthogonal eigenvectors are associated with the same eigenvalue. In the case of non-Hermitian degeneracy, several orthogonal eigenvectors coalesce to a single eigenvector [47]. As a result, the matrix L is not diagonalizable and the exponential e^{Lt} cannot be expressed using the eigenvalue decomposition.

The exponential of a nondiagonalizable matrix L can be expressed using its Jordan normal form: $L = TJT^{-1}$. Here, J is a Jordan-blocks matrix which has (at least) one nondiagonal Jordan block, $J_i = \lambda_i I + N$, where I is the identity and N has ones on its first upper off-diagonal. The exponential of L is expressed as

$$e^{Lt} = Te^{Jt}T^{-1}. \tag{A4}$$

The exponential of the block J_i in e^{Jt} will have the form

$$e^{J_i t} = e^{\lambda_i It + Nt} = e^{\lambda_i t}e^{Nt}. \tag{A5}$$

The matrix N is nilpotent and therefore the Taylor series of e^{Nt} is finite, resulting in a polynomial in the matrix Nt. This gives rise to a polynomial behavior of the solution, and the dynamics of expectation values of operators will have the analytical form of

$$\langle X(t)\rangle = \sum_k \sum_{\alpha=0}^{r_k} d_{k,\alpha} t^\alpha \exp\left[-i\omega_k^{(r_k)} t\right], \tag{A6}$$

instead of the form of Eq. (A3). Here, $\omega_k^{(r_k)}$ denotes a frequency with multiplicity of $r_k + 1$. Note that for nondegenerate frequencies, i.e., $r_k = 0$, we have $d_{k,0} = d_k$ and $\omega_k^{(0)} = \omega_k$. The difference in the analytic behavior of the dynamics results in non-Lorentzian line shapes, with higher-order poles in the complex spectral domain. The point in the spectrum where the eigenvectors coalesce is known as an *exceptional point* (EP).

APPENDIX B: SEARCHING FOR EPs AT THE PARAMETER SPACE

Given a parameter-dependent matrix, the task is to find the exceptional points, i.e., to calculate the parameter set for which the matrix is not diagonalizable.

1. Condition number of an eigenvalue

The diagonalization of matrices in the vicinity of a defective matrix is extremely sensitive to perturbations. The sensitivity of the diagonalization can be characterized by the condition numbers of its eigenvalues. Therefore, the divergence of the condition number of an eigenvalue can be used to find exceptional points. The condition number of an eigenvalue λ of a matrix A with y and x as the corresponding (normalized) left and right eigenvectors, respectively, is defined by

$$\kappa(\lambda, A) = \frac{1}{y^H x}, \tag{B1}$$

where y^H is the Hermitian transpose of y [42,55,56]. At exceptional points, the left and right eigenvectors are perpendicular and the scalar product $y^H x$ vanishes, leading to divergence of the eigenvalue condition number. The condition number of the eigenvalues is implemented in the MATLAB function CONDEIG.

2. Newton methods

There are a couple of methods that use the special properties of the exceptional points in order to find them iteratively:

(a) Mailybaev developed a Newton method of finding multiple eigenvalues with one Jordan block and the corresponding generalized eigenvectors for matrices dependent on parameters. The method computes the nearest value of a parameter vector with a matrix having a multiple eigenvalue of given multiplicity [57]. This method worked well for us in some cases, but failed to find points in which two different eigenvalues had double multiplicity.

(b) Akinola and co-workers used an implicit determinant method to obtain a numerical technique for the calculation of a two-dimensional Jordan block in a parameter-dependent matrix [58].

3. The MFRD method for finding a double eigenvalue of a parameter-dependent matrix

Jarlebring and co-workers suggested a method that for a given two $n \times n$ matrices, A and B, computes all pairs (λ, μ) such that λ is a double eigenvalue of $A + \mu B$ [41]. The method they suggest is the method of fixed relative distance (MFRD). It is based on the assumption that in the vicinity of the double eigenvalue (i.e., for close enough μ), there are two close eigenvalues λ and $(1+\epsilon)\lambda$. In order to find such λ and μ, we have to solve the following coupled eigenvalue equations:

$$(A + \mu B)u = \lambda u, \tag{B2}$$

$$(A + \mu B)v = \lambda(1+\epsilon)v, \tag{B3}$$

where I is the $n \times n$ identity matrix. This kind of problem is called "the two-parameter eigenvalue problem." The most common way to solve and analyze two-parameter eigenvalue problems is by means of three so-called matrix determinants,

$$\Delta_0 = -I \otimes B + (1+\epsilon) B \otimes I, \tag{B4}$$

$$\Delta_1 = -A \otimes B + B \otimes A, \tag{B5}$$

$$\Delta_2 = I \otimes A - (1+\epsilon) A \otimes I. \tag{B6}$$

These are $n^2 \times n^2$ matrices. After constructing these matrices, we solve the following generalized eigenvalues problems:

$$\lambda \Delta_0 z = \Delta_1 z, \tag{B7}$$

$$\mu \Delta_0 z = \Delta_2 z, \tag{B8}$$

to get the approximation for μ and λ and a tensor product $z = u \otimes v$.

The value of ϵ has to be small in order to reflect the double eigenvalue, but not too small in order to maintain stability. As a rule of thumb, a good choice is

$$\epsilon \sim \epsilon_{\text{mach}}^{1/3}, \tag{B9}$$

where ϵ_{mach} is the machine precision.

To summarize, the steps of the method are as follows. Given two $n \times n$ matrices A and B,

(1) Choose appropriate ϵ [see Eq. (B9)]. For $\epsilon_{\text{mach}} = 2.2 \times 10^{-16}$ (MATLAB), we have $\epsilon_{\text{mach}}^{1/3} \approx 6 \times 10^{-6}$.

(2) Construct the matrix determinants of Eqs. (B4)–(B6).

(3) Solve the generalized eigenvalues given by the Eqs. (B7) and (B8) problem to get the approximation for μ and λ.

By construction, this method yields only an approximation of the pairs (λ, μ). But this approximation can be an initial guess for an iterative method or an exact one to get an exact pair (λ, μ).

APPENDIX C: NOISE SENSITIVITY OF THE HARMONIC INVERSION

Parameter estimation naturally raises the issue of sensitivity to noisy experimental data. The noise sensitivity will be determined by the method of harmonic inversion. If the sampling periods have high accuracy, then the time series can be shown to have an underlying Hamiltonian generator. This is the basis for linear methods, such as filter diagonalization (FD) [18,19]. The noise in these methods results in normally distributed underlying matrices, and the model displays monotonous behavior with respect to the noise. This was verified analytically and by means of simulations in Ref. [59]. As a result, sufficient averaging will eliminate the noise. Practical implementations require further analysis with evidence of nonlinear effects of noise. For example, Mandelshtam *et al.* analyzed the noise sensitivity of the FD in the context of NMR experiments [21,60] and Fourier-transform mass spectrometry [22]. For some other methods, a noise-reduction technique was proposed in Ref. [20].

[1] H. Katori, Optical lattice clocks and quantum metrology, Nat. Photon. **5**, 203 (2011).

[2] A. D. Ludlow, M. M. Boyd, J. Ye, E. Peik, and P. O. Schmidt, Optical atomic clocks, Rev. Mod. Phys. **87**, 637 (2015).

[3] K. Matsubara, H. Hachisu, Y. Li, S. Nagano, C. Locke, A. Nogami, M. Kajita, K. Hayasaka, T. Ido, and M. Hosokawa, Direct comparison of a single-ion clock against a sr lattice clock to verify the absolute frequency measurement, Opt. Express **20**, 22034 (2012).

[4] N. R. Nand, J. G. Hartnett, E. N. Ivanov, and G. Santarelli, Ultra-stable very-low phase-noise signal source for very long baseline interferometry using a cryocooled sapphire oscillator, IEEE Trans. Microwave Theory Techn. **59**, 2978 (2011).

[5] C.-W. Chou, D. B. Hume, T. Rosenband, and D. J. Wineland, Optical clocks and relativity, Science **329**, 1630 (2010).

[6] S. Blatt, A. D. Ludlow, G. K. Campbell, J. W. Thomsen, T. Zelevinsky, M. M. Boyd, J. Ye, X. Baillard, M. Fouché, R. L. Targat *et al.*, New Limits on Coupling of Fundamental Constants to Gravity Using ^{87}Sr Optical Lattice Clocks, Phys. Rev. Lett. **100**, 140801 (2008).

[7] P. J. Mohr, B. N. Taylor, and D. B. Newell, The 2010 codata recommended values of the fundamental physical constants, Web version, 6(2), 2011 (unpublished).

[8] R. Pohl, A. Antognini, F. Nez, F. D. Amaro, F. Biraben, J. M. R. Cardoso, D. S. Covita, A. Dax, S. Dhawan, L. M. P. Fernandes *et al.*, The size of the proton, Nature (London) **466**, 213 (2010).

[9] M. Chaichian, M. M. Sheikh-Jabbari, and A. Tureanu, Hydrogen Atom Spectrum and the Lamb Shift in Noncommutative QED, Phys. Rev. Lett. **86**, 2716 (2001).

[10] C. Itzykson and J.-B. Zuber, *Quantum Field Theory* (Dover Publications, New York, 2006).

[11] G. S. Agarwal, Master-equation approach to spontaneous emission, Phys. Rev. A **2**, 2038 (1970).

[12] C. Cohen-Tannoudji, J. Dupont-Roc, and G. Grynberg, *Atom-photon Interactions: Basic Process and Applications* (Wiley-VCH, New York, 1998), pp. 353–405.

[13] G. Lindblad, On the generators of quantum dynamical semigroups, Commun. Math. Phys. **48**, 119 (1976).

[14] V. Gorini, A. Kossakowski, and E. C. G. Sudarshan, Completely positive dynamical semigroups of n-level systems, J. Math. Phys. **17**, 821 (1976).

[15] H.-P. Breuer and F. Petruccione, *The Theory of Open Quantum Systems* (Oxford University Press, Oxford, 2002).

[16] R. Alicki and M. Fannes, *Quantum Dynamical Systems* (Oxford University Press, Oxford, 2001).

[17] M. Am-Shallem, A. Levy, I. Schaefer, and R. Kosloff, Three approaches for representing Lindblad dynamics by a matrix-vector notation, arXiv:1510.08634.

[18] M. R. Wall and D. Neuhauser, Extraction, through filter-diagonalization, of general quantum eigenvalues or classical normal mode frequencies from a small number of residues or a short-time segment of a signal. i. theory and application

to a quantum-dynamics model, J. Chem. Phys. **102**, 8011 (1995).
[19] V. A. Mandelshtam, FDM: the filter diagonalization method for data processing in nmr experiments, Prog. Nucl. Magn. Reson. Spectrosc. **38**, 159 (2001).
[20] Dž. Belkić, P. A. Dando, J. Main, and H. S. Taylor, Three novel high-resolution nonlinear methods for fast signal processing, J. Chem. Phys. **113**, 6542 (2000).
[21] H. Hu, Q. N. Van, V. A. Mandelshtam, and A. J. Shaka, Reference deconvolution, phase correction, and line listing of NMR spectra by the 1d filter diagonalization method, J. Magn. Reson. **134**, 76 (1998).
[22] B. R. Martini, K. Aizikov, and V. A. Mandelshtam, The filter diagonalization method and its assessment for Fourier transform mass spectrometry, Intl. J. Mass Spectrosc. **373**, 1 (2014).
[23] E. Gershgoren, J. Vala, R. Kosloff, and S. Ruhman, Impulsive control of ground surface dynamics of I_3^- in solution, J. Phys. Chem. A **105**, 5081 (2001).
[24] J. Fuchs, J. Main, H. Cartarius, and G. Wunner, Harmonic inversion analysis of exceptional points in resonance spectra, J. Phys. A: Math. Theor. **47**, 125304 (2014).
[25] M. Am-Shallem, R. Kosloff, and N. Moiseyev, Exceptional points for parameter estimation in open quantum systems: Analysis of the Bloch equations, New J. Phys. **17**, 113036 (2015).
[26] Daniel A. Steck, Rubidium 85 D Line Data, available online at http://steck.us/alkalidata (revision 2.1.6, 20 September 2013).
[27] M. Ramm, T. Pruttivarasin, M. Kokish, I. Talukdar, and H. Häffner, Precision Measurement Method for Branching Fractions of Excited $P_{1/2}$ States Applied to $^{40}Ca^+$, Phys. Rev. Lett. **111**, 023004 (2013).
[28] C. Roos, Quantum information processing with trapped ions, in *Fundamental Physics in Particle Traps*, Springer Tracts in Modern Physics, Vol. 256, edited by W. Quint and M. Vogel (Springer, Berlin Heidelberg, 2014), pp. 253–291.
[29] J. T Barreiro, P. Schindler, O. Gühne, T. Monz, M. Chwalla, C. F. Roos, M. Hennrich, and R. Blatt, Experimental multiparticle entanglement dynamics induced by decoherence, Nat. Phys. **6**, 943 (2010).
[30] P. Schindler, D. Nigg, T. Monz, J. T. Barreiro, E. Martinez, S. X. Wang, S. Quint, M. F. Brandl, V. Nebendahl, C. F. Roos, M. Chwalla, M. Hennrich, and R. Blatt, A quantum information processor with trapped ions, New J. Phys. **15**, 123012 (2013).
[31] M. Harlander, R. Lechner, M. Brownnutt, R. Blatt, and W. Hänsel, Trapped-ion antennae for the transmission of quantum information, Nature (London) **471**, 200 (2011).
[32] S. A. Schulz, U. Poschinger, F. Ziesel, and F. Schmidt-Kaler, Sideband cooling and coherent dynamics in a microchip multi-segmented ion trap, New J. Phys. **10**, 045007 (2008).
[33] U. Poschinger, A. Walther, M. Hettrich, F. Ziesel, and F. Schmidt-Kaler, Interaction of a laser with a qubit in thermal motion and its application to robust and efficient readout, Appl. Phys. B **107**, 1159 (2012).
[34] K. Gao, Optical frequency standard based on a single $^{40}Ca^+$, Chin. Sci. Bull. **58**, 853 (2013).
[35] H. Guan, Y. Huang, P.-L. Liu, W. Bian, H. Shao, and K.-L. Gao, Precision spectroscopy with a single $^{40}Ca^+$ ion in a paul trap, Chin. Phys. B **24**, 054213 (2015).
[36] P.-L. Liu, Y. Huang, W. Bian, H. Shao, H. Guan, Y.-B. Tang, C.-B. Li, J. Mitroy, and K.-L. Gao, Measurement of Magic Wavelengths for the $^{40}Ca^+$ Clock Transition, Phys. Rev. Lett. **114**, 223001 (2015).
[37] A. L. Wolf, J. Morgenweg, J. C. J. Koelemeij, S. A. van den Berg, W. Ubachs, and K. S. E. Eikema, Direct frequency-comb spectroscopy of a dipole-forbidden clock transition in trapped $^{40}Ca^+$ ions, Opt. Lett. **36**, 49 (2011).
[38] J. Roßnagel, S. T. Dawkins, K. N. Tolazzi, O. Abah, E. Lutz, F. Schmidt-Kaler, and K. Singer, A single-atom heat engine, arXiv:1510.03681.
[39] A. L. Wolf, S. A. van den Berg, C. Gohle, E. J. Salumbides, W. Ubachs, and K. S. E. Eikema, Frequency metrology on the $4s^2S_{1/2} - 4p^2P_{1/2}$ transition in $^{40}Ca^+$ for a comparison with quasar data, Phys. Rev. A **78**, 032511 (2008).
[40] A. L. Wolf, S. A. van den Berg, W. Ubachs, and K. S. E. Eikema, Direct Frequency Comb Spectroscopy of Trapped Ions, Phys. Rev. Lett. **102**, 223901 (2009).
[41] E. Jarlebring, S. Kvaal, and W. Michiels, Computing all pairs (λ, μ) such that λ is a double eigenvalue of $a + \mu b$, SIAM J. Matrix Anal. Appl. **32**, 902 (2011).
[42] F. Chatelin, *Spectral Approximation of Linear Operators* (SIAM, Philadelphia, 2011), Chap. 1, pp. 1–65.
[43] R. Alicki, Invitation to quantum dynamical semigroups, in *Dynamics of Dissipation*, Lecture Notes in Physics, Vol. 597 (Springer, Berlin Heidelberg, 2002), pp. 239–264.
[44] R. Alicki and K. Lendi, *Quantum Dynamical Semigroups and Applications*, Lecture Notes in Physics, Vol. 717 (Springer, Berlin, Heidelberg, 2007).
[45] M. A. Nielsen and I. L. Chuang, *Quantum Computation and Quantum Information: 10th Anniversary Edition* (Cambridge University Press, NY, 2011).
[46] M. Müller and I. Rotter, Exceptional points in open quantum systems, J. Phys. A: Math. Theor. **41**, 244018 (2008).
[47] N. Moiseyev, *Non-Hermitian Quantum Mechanics* (Cambridge University Press, Cambridge, 2011).
[48] J.-W. Ryu, S.-Y. Lee, and S. W. Kim, Analysis of multiple exceptional points related to three interacting eigenmodes in a non-Hermitian Hamiltonian, Phys. Rev. A **85**, 042101 (2012).
[49] W. D. Heiss, Chirality of wave functions for three coalescing levels, J. Phys. A: Math. Theor. **41**, 244010 (2008).
[50] G. Demange and E.-M. Graefe, Signatures of three coalescing eigenfunctions, J. Phys. A: Math. Theor. **45**, 025303 (2012).
[51] W. D. Heiss and G. Wunner, Resonance scattering at third-order exceptional points, J. Phys. A: Math. Theor. **48**, 345203 (2015).
[52] W. D. Heiss, Green's functions at exceptional points. Intl. J. Theor. Phys. **54**, 3954 (2015).
[53] H. Cartarius, J. Main, and G. Wunner, Exceptional points in the spectra of atoms in external fields, Phys. Rev. A **79**, 053408 (2009).
[54] M. Am-Shallem and R. Kosloff, The scaling of weak field phase-only control in markovian dynamics, J. Chem. Phys. **141**, 044121 (2014).
[55] G. H. Golub and C. F. Van Loan, *Matrix Computations. Johns Hopkins Series in the Mathematical Sciences* (Johns Hopkins University Press, Baltimore, MD, 1989).
[56] C. Moler, *Numerical Computing with Matlab* (SIAM, Philadelphia, 2004), Chap. 10, pp. 269–305.

[57] A. A. Mailybaev, Computation of multiple eigenvalues and generalized eigenvectors for matrices dependent on parameters, Numer. Linear Algebra Appl. **13**, 419 (2006).

[58] R. O. Akinola, M. A. Freitag, and A. Spence, The computation of Jordan blocks in parameter-dependent matrices, IMA J. Numer. Anal. **34**, 955 (2014).

[59] U. Benko and Đ. Juričić, Frequency analysis of noisy short-time stationary signals using filter-diagonalization, Signal Proc. **88**, 1733 (2008).

[60] H. Celik, A. J. Shaka, and V. A. Mandelshtam, Sensitivity analysis of solutions of the harmonic inversion problem: Are all data points created equal?, J. Magn. Reson. **206**, 120 (2010).